Available online at www.sciencedirect.com
ScienceDirect
Journal of the Mechanics and Physics of Solids 56 (2008) 2459–2472
JOURNAL OF THE MECHANICS AND PHYSICS OF SOLIDS
www.elsevier.com/locate/jmps

Fracture toughness from the standpoint of softening hyperelasticity

K.Y. Volokh*, P. Trapper

Faculty of Civil and Environmental Engineering, Technion-I.I.T., Haifa 32000, Israel

Received 12 October 2007; accepted 28 February 2008

Abstract

Fracture toughness of brittle materials is calibrated in experiments where a sample with a preexisting crack/notch is loaded up to a critical point of the onset of static instability. Experiments with ceramics, for example, exhibit a pronounced dependence of the toughness on the sharpness of the crack/notch: the sharper is the crack the lower is the toughness. These experimental results are not entirely compatible with the original Griffith theory of brittle fracture where the crack sharpness is of minor importance.[1]

To explain the experimental observations qualitatively we simulate tension of a thin plate with a small crack of a finite and varying sharpness. In simulations, we introduce the average bond energy as a limiter for the stored energy of the Hookean solid. The energy limiter induces softening, indicating material failure. Thus, elasticity with softening allows capturing the critical point of the onset of static instability of the cracked plate, which corresponds to the onset of the failure propagation at the tip of the crack. In numerical simulations we find, in agreement with experiments, that the magnitude of the fracture toughness cannot be determined uniquely because it depends on the sharpness of the crack: the sharper is the crack, the lower is the toughness.

Based on the obtained results, we argue that a stable magnitude of the toughness of brittle materials can only be reached when a characteristic size of the crack tip is comparable with a characteristic length of the material microstructure, e.g. grain size, atomic distance, etc. In other words, the toughness can be calibrated only under conditions where the hypothesis of continuum fails.

Keywords: Fracture; Toughness; Softening hyperelasticity; Material failure

1. Introduction

Toughness calibration is tough. The problem is that the experimental results soundly depend on the sharpness of a *real* notch/crack: Bertolotti (1973), Myers and Hillberry (1977), Munz et al. (1980), Wang et al. (1992), Tsuji et al. (1999), Gogotsi (2003), and Yosibash et al. (2004). These experimental results are not

*Corresponding author.
E-mail address: cvolokh@technion.ac.il (K.Y. Volokh).

[1]The finite sharpness of real cracks is also ignored in the modern theory of Linear Elastic Fracture Mechanics where 'mathematical' cracks with zero width and tip singularity are considered.

0022-5096/$ - see front matter © 2008 Elsevier Ltd. All rights reserved.
doi:10.1016/j.jmps.2008.02.009

entirely compatible with the original Griffith theory of brittle fracture where the crack sharpness is of no influence. Indeed, considering a plane with a central elliptic crack under the remote hydrostatic tension and using the energy balance Griffith (1921) derived the following formula for the critical tension[2]:

$$p_{\mathrm{cr}} = \sqrt{\frac{8\mu G_{\mathrm{Ic}}}{(1+k)\pi c \cosh(2\alpha_0)}}. \tag{1}$$

Here the 'crack length', $2c$, is formally related with the ellipse semi-axes along the crack, a, and orthogonal to the crack, b, by formula $c^2 = a^2 - b^2$. It is assumed that the ellipse is crack-like, i.e. $a \gg b$, and consequently, $c \approx a$. The shear modulus is $\mu = E/2(1+\nu)$ where the Young modulus and Poisson ratio are E and ν accordingly. The constant of the stress/strain state is $k = 3-4\nu$ in the case of plane strain and $k = (3-\nu)/(1+\nu)$ in the case of plane stress. The critical (Mode I) energy release rate, G_{Ic}, equals twice the Griffith surface tension, γ: $G_{\mathrm{Ic}} = 2\gamma$. Finally, α_0 is the elliptic coordinate of the crack. We notice that the crack sharpness is included in the critical force through the hyperbolic cosine, which is related with the crack axes as follows:

$$\cosh(2\alpha_0) = \frac{a^2 + b^2}{a^2 - b^2} \approx 1, \tag{2}$$

where the approximate equality is a consequence of the crack geometry, i.e. $a \gg b$.

Substituting Eq. (2) in Eq. (1) we have finally:

$$p_{\mathrm{cr}} = \sqrt{\frac{8\mu G_{\mathrm{Ic}}}{(1+k)\pi a}}. \tag{3}$$

It is crucial to note that the Griffith critical load is practically unaffected by the sharpness of the crack tip because of Eq. (2).

Analogously to Griffith, the modern theory of Linear Elastic Fracture Mechanics (LEFM) ignores the real crack sharpness yet in a more sophisticated way—it considers 'mathematical' cracks with zero width and tip singularity: Broberg (1999), Hellan (1984), Hertzberg (1989), Kanninen and Popelaar (1973). According to LEFM, the critical tension in a plate with central crack of length $2a$ is given by:

$$p_{\mathrm{cr}} = \frac{K_{\mathrm{Ic}}}{\sqrt{\pi a}}, \tag{4}$$

where $K_{\mathrm{Ic}} = \sqrt{8\mu G_{\mathrm{Ic}}/(1+k)}$ is the Mode I fracture toughness or the critical stress intensity factor (SIF). Expectedly, Eqs. (3) and (4) coincide.

There is an evident mismatch between the experimental importance of the crack sharpness and its theoretical ignorance—see also Doremus (1976). To shed more light on this controversy, we study the Griffith problem theoretically without using the classical fracture theories. Instead, we simulate failure of a cracked plate by using the softening hyperelasticity approach described in Section 2. Such an approach allows capturing the critical load on the cracked plate, which corresponds to the onset of static instability. Thus, our theoretical study is essentially a series of numerical experiments. The numerical experiments are not affected by the problems accompanying the physical experiments and because of that they can be a valuable source of additional information.

We plug the softening hyperelasticity models in ABAQUS and use very fine meshes to simulate small cracks with the varying sharpness or length in Section 3. We find that the crack sharpness affects the onset of plate failure and, consequently, the fracture toughness in perfect qualitative agreement with the physical experiments.

We discuss the results of our simulations and the classical theories of brittle fracture in Section 4. Particularly, we argue that the ignorance of the crack sharpness in the classical fracture theories is related to the energetic nature of these theories. The latter means that the energy balance, which is an integral equation, 'smears' the stress/strain concentration at the tip of the crack making the theory insensitive to the crack sharpness. The smearing appears explicitly in the original Griffith theory and it is implicit in LEFM. We also

[2]Originally, Griffith writes $(3-k)$ instead of the correct $(1+k)$.

argue that the measurements of the fracture toughness can converge to stable values only in the cases where the radius of the crack tip is comparable with a characteristic size of the material microstructure, e.g. grain size, atomic distance, etc., corresponding, for example, to the Emmerich (2007) parameter λ_a that represents the minimum characteristic length scale round the point where the fracture begins. In other words, the toughness can be calibrated only under conditions where the hypothesis of continuum fails. The latter means, for example, that the measurements of the ceramics toughness with the notch radius significantly larger than the grain size may be hopeless in advance.

2. Softening hyperelasticity

2.1. Preliminary remarks

The existing continuum mechanics approaches for modeling material failure can be divided in two groups: surface and bulk models. The surface models, pioneered by Barenblatt (1959), appear by name of cohesive zone models (CZM) in the modern literature. The cohesive zone is a surface in a bulk material where displacement discontinuities occur. Thus, continuum is enhanced with discontinuities. The latter requires an additional constitutive description. Equations relating normal and tangential displacement jumps across the cohesive surfaces with the proper tractions define a specific CZM. There is a plenty of proposals of the 'cohesive' constitutive equations, for example, Dugdale (1960), Rice and Wang (1989), Tvergaard and Hutchinson (1992), Xu and Needleman (1994), and Camacho and Ortiz (1996). All these models are constructed qualitatively as follows: tractions increase, reach a maximum, and then approach zero with increasing separation. This scenario is in harmony with our intuitive understanding of the rupture process. Needleman (1987) lifted the CZMs to computational practice. Since then CZMs are used increasingly in finite element simulations of crack tip plasticity and creep, crazing in polymers, adhesively bonded joints, interface cracks in bimaterials, delamination in composites and multilayers, fast crack propagation in polymers, etc. Cohesive zones can be inside finite elements or along their boundaries (de Borst, 2001; Xu and Needleman, 1994; Belytschko et al., 2001). Crack nucleation, propagation, branching, kinking, and arrest are a natural outcome of the computations where the discontinuity surfaces are spread over the bulk material. This is in contrast to the traditional approach of fracture mechanics where stress analysis is separated from a description of the actual process of material failure. The CZM approach is natural for simulation of fracture at the *internal material interfaces* in polycrystals, composites, and multilayers. It is less natural for modeling fracture of the bulk because it leads to the simultaneous use of two material models for the same real material: one model describes the bulk while the other model describes the cohesive zones imbedded in the bulk. Such two-model approach is rather artificial physically. It seems preferable to incorporate a material failure law directly in the constitutive description of the bulk.

Remarkably, the first models of bulk failure—damage mechanics—proposed by Kachanov (1958) and Rabotnov (1963) for analysis of the gradual failure accumulation and propagation in *creep* and *fatigue* appeared almost simultaneously with the cohesive zone approach. The need to describe the failure accumulation, i.e. evolution of the material microstructure, explains why damage mechanics is very similar to plasticity theories including (a) the internal damage variable (inelastic strain), (b) the critical threshold condition (yield surface), and (c) the damage evolution equation (flow rule). The subsequent development of the formalism of damage mechanics (Kachanov, 1986; Krajcinovic, 1996; Skrzypek and Ganczarski, 1999; Lemaitre and Desmorat, 2005) left its physical origin well behind the mathematical and computational techniques and eventually led to the use of damage mechanics for the description of *any* bulk failure. Theoretically, the approach of damage mechanics is very flexible and allows reflecting the physical processes triggering macroscopic damage at small length scales. Practically, the experimental calibration of damage theories is far from trivial because it is difficult to measure the damage parameter directly. The experimental calibration should be implicit and include both the damage evolution equation and criticality condition.

A physically motivated alternative to damage mechanics in the cases of failure related with the bond rupture has been considered by Gao and Klein (1998), Klein and Gao (1998), and, more recently, by Volokh and Gao (2005), who showed how to mix the atomic/molecular and continuum descriptions in order to simulate material failure. They applied the Cauchy-Born rule linking micro- and macro-scales to empirical potentials,

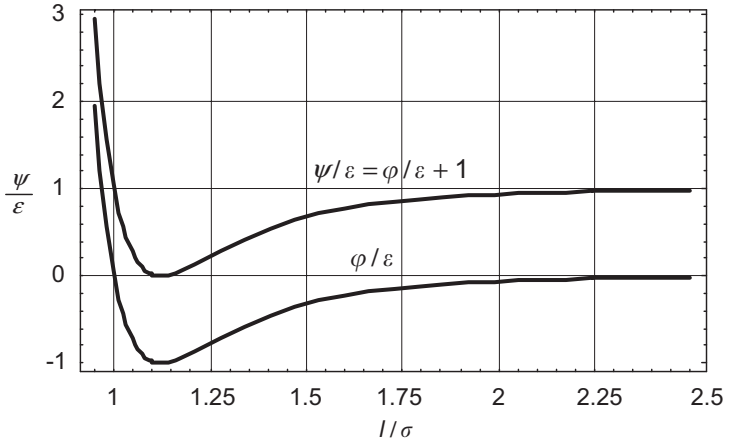

Fig. 1. Lennard-Jones potential.

which include a possibility of the full atomic separation. The continuum–atomistic link led to the formulation of the macroscopic strain energy potentials allowing for the stress/strain softening and strain localization. The continuum–atomistic method is very effective at small length scales where purely atomistic analysis becomes computationally intensive. This approach found applications in bio- and nano-mechanics concerning the problems of bone fracture (Gao et al., 2003; Ji and Gao, 2004) and strength of carbon nanotubes (Zhang et al., 2004; Volokh and Ramesh, 2006). Unfortunately, a direct use of the continuum–atomistic method in macroscopic failure problems is not very feasible because its computer implementation includes a numerically involved procedure of the averaging of the interatomic potentials over a representative volume.

In order to bypass the computational intensity of the continuum–atomistic method while preserving its sound physical basis, the *softening hyperelasticity* approach was proposed by Volokh (2004, 2007a, b). The basic idea of the approach is to formulate an expression of the stored macroscopic energy, which includes the energy limiter—the average bond energy.[3] Such a limiter introduces the strain softening, i.e. the material failure description, in constitutive equations of continuum mechanics automatically. The softening hyperelasticity approach is computationally simple yet physically appealing and its application to the simulation of the onset of the crack propagation in brittle solids is considered in the present work. It is interesting that the existence of an energy limiter has been observed by Rittel et al. (2006) in experiments on adiabatic shear failure.

2.2. Energy limiter for a pair of particles

Let us start with the interaction of two particles (atoms, molecules, etc.) and let us choose, to be specific, the Lennard-Jones potential, φ, for the description of the particle interaction:

$$\varphi(l) = 4\varepsilon\left(\left(\frac{\sigma}{l}\right)^{12} - \left(\frac{\sigma}{l}\right)^{6}\right), \tag{5}$$

where l is the distance between particles, ε and σ are the *bond energy* and length constants, respectively (Fig. 1).

Let L designate the distance between particles in a reference state and F is the one-dimensional deformation gradient. In the latter case we have:

$$l = FL. \tag{6}$$

Substituting Eq. (6) in Eq. (7) we have:

$$\varphi(F) = 4\varepsilon\left(\left(\frac{\sigma}{FL}\right)^{12} - \left(\frac{\sigma}{FL}\right)^{6}\right). \tag{7}$$

[3]In the case of continuum–atomistic methods, the energy limiter is already embedded in the description of individual bonds.

Assuming that deformation increases to infinity we have:

$$\varphi(F \to \infty) = 0. \tag{8}$$

On the other hand, we have at the reference state:

$$\varphi_0 = \varphi(F = 1) = 4\varepsilon\left(\left(\frac{\sigma}{L}\right)^{12} - \left(\frac{\sigma}{L}\right)^{6}\right). \tag{9}$$

In the absence of external loads the energy of the interaction tends to minimum and it is natural to choose the minimum energy state—equilibrium—at distance $L = \sqrt[6]{2}\sigma$ where no forces are acting between the particles. In the latter case, we have:

$$\varphi_0 = -\varepsilon. \tag{10}$$

We notice that energy is negative in the equilibrium state according to the classical Lennard-Jones potential. The latter is inconvenient (in problems of solid mechanics) and we modify the classical LJ potential by shifting its reference energy to zero (Fig. 1)

$$\psi = \varphi + \varepsilon. \tag{11}$$

We further formalize the described energy shift as follows:

$$\psi(F) = \varphi(F) - \varphi_0, \tag{12}$$

$$\varphi_0 = \min_L \varphi(F = 1). \tag{13}$$

Eqs. (12) and (13) are important in the subsequent consideration of assemblies of many particles.

It is important to emphasize that we cannot increase energy unlimitedly by increasing deformation. The energy increase is limited:

$$\psi(F \to \infty) = -\varphi_0 = \Phi = \text{constant}. \tag{14}$$

2.3. Energy limiter for assembly of particles

Now we extend all considerations for a pair of particles given in the previous subsection to large particle assemblies comprising solid bodies. Consider particles placed at $\mathbf{r}_i$ in the 3D space. Generally, the volumetric density of the total potential energy, i.e. the strain energy, can be written with account of two-particle interactions as follows:

$$\frac{1}{2V}\sum_{i,j}\varphi(r_{ij}), \tag{15}$$

where $r_{ij} = |\mathbf{r}_{ij}| = |\mathbf{r}_i - \mathbf{r}_j|$ and V is the volume occupied by the system.

According to the Cauchy-Born rule (Weiner, 1983; Tadmor et al., 1996), originally applied to the crystal elasticity, the current $\mathbf{r}_{ij}$ and initial (reference) $\mathbf{R}_{ij} = \mathbf{R}_i - \mathbf{R}_j$ relative positions of the same two particles can be related by the deformation gradient:

$$\mathbf{r}_{ij} = \mathbf{F}\mathbf{R}_{ij}, \tag{16}$$

where $\mathbf{F} = \partial\mathbf{x}/\partial\mathbf{X}$ is the deformation gradient of a generic material macro-particle of body Ω occupying position $\mathbf{X}$ at the reference state and position $\mathbf{x}(\mathbf{X})$ at the current state of deformation (Fig. 2).

Substituting Eq. (16) in Eq. (15) yields:

$$\frac{1}{2V}\sum_{i,j}\varphi(r_{ij}) = \frac{1}{2V}\sum_{i,j}\varphi(r_{ij}(\mathbf{C})), \tag{17}$$

where $\mathbf{C} = \mathbf{F}^{\mathrm{T}}\mathbf{F}$ is the right Cauchy-Green deformation tensor.

Direct application of Eq. (17) to analysis of material behavior can be difficult because of the large amount of particles. Gao and Klein (1998) and Klein and Gao (1998, 2000) considered the following statistical averaging

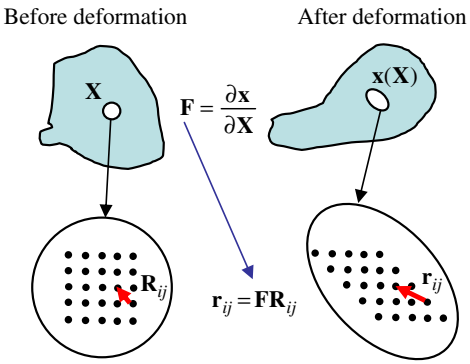

Fig. 2. Cauchy-Born rule.

procedure:

$$\langle\varphi(l)\rangle = \frac{1}{V_0}\int_{V_0^*}\varphi(l)D_{\mathrm{V}}\,\mathrm{d}V, \tag{18}$$

$$l = r_{ij} = L\sqrt{\boldsymbol{\xi}\cdot\mathbf{C}\boldsymbol{\xi}} = L|\mathbf{F}\boldsymbol{\xi}|, \tag{19}$$

where $L = R_{ij} = |\mathbf{R}_i - \mathbf{R}_j|$ is the reference bond length; $\boldsymbol{\xi} = (\mathbf{R}_i - \mathbf{R}_j)/L$ is the reference bond direction; V_0 is the reference representative volume; $\varphi(l)$ is the bond potential (Lennard-Jones); D_{V} is the volumetric bond density function; and V_0^* is the integration volume defined by the range of influence of φ.

Now the average strain energy takes the form:

$$\langle\varphi(\mathbf{C})\rangle = \frac{1}{V_0}\int_{V_0^*} 4\varepsilon\left(\left(\frac{\sigma}{L||\mathbf{C}||}\right)^{12} - \left(\frac{\sigma}{L||\mathbf{C}||}\right)^{6}\right)D_{\mathrm{V}}\,\mathrm{d}V, \tag{20}$$

where

$$||\mathbf{C}|| = \sqrt{\boldsymbol{\xi}\cdot\mathbf{C}\boldsymbol{\xi}}. \tag{21}$$

Analogously to the case of the pair interaction considered in the previous subsection—Eqs. (12) and (13)—we define the shifted strain energy, which is zero at the equilibrium reference state:

$$\psi(\mathbf{C}) = \langle\varphi(\mathbf{C})\rangle - \langle\varphi\rangle_0, \tag{22}$$

$$\langle\varphi\rangle_0 = \min_L\langle\varphi(\mathbf{C} = \mathbf{1})\rangle. \tag{23}$$

Analogously to Eq. (14), we can define *the average bond energy* by setting the unlimited increase of deformation:

$$\Phi = \psi(||\mathbf{C}|| \to \infty) = -\langle\varphi\rangle_0 = \text{constant}. \tag{24}$$

Thus, the average bond energy sets a limit for the energy accumulation. This conclusion generally does not depend on the choice of the particle potential and it is valid for any interaction that includes a possible particle separation—the bond energy.

2.4. Energy limiter for a solid

Contrary to the conclusion above, traditional hyperelastic models of materials do not include the energy limiter. The stored energy of hyperelastic materials is defined as:

$$\psi = W. \tag{25}$$

Here, W is used for the strain energy of the *intact* material, which can be characterized as follows:

$$||\mathbf{C}|| \to \infty \Rightarrow \psi = W \to \infty, \tag{26}$$

where $||\mathbf{C}||$ is a tensorial norm.

In other words, the increasing strain increases the accumulated energy unlimitedly. Evidently, the consideration of only intact materials is restrictive and unphysical. The energy increase of a real material should be limited as it was shown above:

$$\|\mathbf{C}\| \to \infty \Rightarrow \psi \to \Phi = \text{constant}, \tag{27}$$

where the average bond energy, $\Phi = \text{constant}$, can be called the *material failure energy*.

Eq. (27) presents the fundamental idea of introducing a limiter of the stored energy in the elasticity theory. Such a limiter induces material softening, indicating material failure, automatically. The choice of the limited stored energy expression should generally be material-specific. Nonetheless, a somewhat universal formula (Volokh, 2007b) can be introduced to enrich the already existing models of intact materials with the failure description:

$$\psi(W) = \Phi - \Phi \exp\left(-\frac{W}{\Phi}\right). \tag{28}$$

where $\psi(W=0)=0$ and $\psi(W=\infty)=\Phi$.

Formula (28) obeys condition $||\mathbf{C}|| \to \infty \Rightarrow \psi(W(\mathbf{C})) \to \Phi$ and, in the case of the intact material behavior, $W \ll \Phi$, we have $\psi(W) \approx W$ preserving the features of the intact material.

The constitutive equation can be written in the general form accounting for (Eq. (28)):

$$\boldsymbol{\sigma} = 2J^{-1}\mathbf{F}\frac{\partial \psi}{\partial \mathbf{C}}\mathbf{F}^T = 2J^{-1}\mathbf{F}\frac{\partial W}{\partial \mathbf{C}}\mathbf{F}^T \exp\left(-\frac{W}{\Phi}\right), \tag{29}$$

where $\boldsymbol{\sigma}$ is the Cauchy stress tensor; $J = \det \mathbf{F}$; and the exponential multiplier enforces material softening. Constitutive Eq. (29) is especially effective for incompressible soft materials undergoing finite deformations.

2.5. Hookean solid with failure

In the case of linear Hookean solid, which is of interest in the present study, we have for Eqs. (28) and (29) accordingly:

$$\psi = \Phi - \Phi \exp\left(-\frac{\lambda}{2\Phi}(\mathrm{tr}\boldsymbol{\varepsilon})^2 - \frac{\mu}{\Phi}\boldsymbol{\varepsilon} : \boldsymbol{\varepsilon}\right), \tag{30}$$

$$\boldsymbol{\sigma} = \frac{\partial \psi}{\partial \boldsymbol{\varepsilon}} = (2\mu\boldsymbol{\varepsilon} + \lambda(\mathrm{tr}\varepsilon)\mathbf{1}) \exp\left(-\frac{\lambda}{2\Phi}(\mathrm{tr}\boldsymbol{\varepsilon})^2 - \frac{\mu}{\Phi}\boldsymbol{\varepsilon} : \boldsymbol{\varepsilon}\right), \tag{31}$$

where $\boldsymbol{\varepsilon}:\boldsymbol{\varepsilon} = \mathrm{tr}(\boldsymbol{\varepsilon}\boldsymbol{\varepsilon}^{\mathrm{T}})$; λ and μ are the Lame material constants and

$$\boldsymbol{\varepsilon} = \frac{1}{2}\left(\mathbf{H} + \mathbf{H}^T\right) \tag{32}$$

is the linear strain; $\mathbf{1}$ is the second-order identity tensor and $\mathbf{H} = \partial \mathbf{u}/\partial \mathbf{X}$ is the displacement, $\mathbf{u} = \mathbf{x} - \mathbf{X}$, gradient.

Though Eq. (29) presents a universal formula to introduce the average bond energy in consideration, it is by no means unique. It is possible, for example, to introduce the energy limiter for the linear isotropic Hookean solid in the following way (Volokh 2004, 2007a):

$$\psi = \Phi - \Phi\left(1 + \sqrt{\frac{K}{\Phi}}\mathrm{tr}\boldsymbol{\varepsilon}\right) \exp\left(-\sqrt{\frac{K}{\Phi}}\mathrm{tr}\boldsymbol{\varepsilon} - \frac{\mu}{\Phi}\mathbf{e} : \mathbf{e}\right), \tag{33}$$

$$\boldsymbol{\sigma} = \frac{\partial \psi}{\partial \boldsymbol{\varepsilon}} = 2\tilde{\mu}\boldsymbol{\varepsilon} + \left(\tilde{K} - \frac{2\tilde{\mu}}{3}\right)(\mathrm{tr}\boldsymbol{\varepsilon})\mathbf{1}, \tag{34}$$

where

$$\mathbf{e} = \boldsymbol{\varepsilon} - \frac{1}{3}(\mathrm{tr}\boldsymbol{\varepsilon})\mathbf{1}, \tag{35}$$

$$\tilde{\mu} = \mu\left(1 + \sqrt{\frac{K}{\Phi}}\mathrm{tr}\boldsymbol{\varepsilon}\right)\exp\left(-\sqrt{\frac{K}{\Phi}}\mathrm{tr}\boldsymbol{\varepsilon} - \frac{\mu}{\Phi}\mathbf{e}:\mathbf{e}\right), \tag{36}$$

$$\tilde{K} = K\exp\left(-\sqrt{\frac{K}{\Phi}}\mathrm{tr}\boldsymbol{\varepsilon} - \frac{\mu}{\Phi}\mathbf{e}:\mathbf{e}\right), \tag{37}$$

where $K = \lambda + 2\mu/3$ is the bulk modulus.

We emphasize again that the best form of the energy function can be material/problem-specific. It is important, however, that all possible forms should limit the energy increase. In what follows, we will use both Eqs. (30) and (33).

3. Finite element simulations

The purpose of the finite element analysis is to simulate the hydrostatic tension of a thin plate with the *small* elliptic and straight cracks—Fig. 3—under the varying sharpness and length of the cracks.

For this purpose, we use the ABAQUS software where the stored energy functions (30) and (33) are plugged in. Henceforth, we call the material model based on Eq. (33) Softening Hyperelasticity 1—SH1—and on Eq. (30) Softening Hyperelasticity 2—SH2. We consider the state of the plane stress for a square plate of size $d = 1600$ (units) with elastic constants $\lambda/\Phi = 75 \times 10^4/66$ and $\mu/\Phi = 90 \times 10^4/66$. We use very fine meshes of triangles and quadrilaterals as shown in Fig. 4. The number of elements varies for various loading cases. We consider three series of simulations in the subsequent subsections.

3.1. Elliptic crack with varying sharpness

We start with the elliptic crack simulation with fixed length of $2a = 80$ (units) and varying sharpness, i.e. the 'width' half axes of the elliptic crack: $b = 1, 2, 3, 4, 5, 6, 7, 8$ (units). Table 1 presents the normalized critical tension for eight cases of the crack sharpness.

Every case is simulated eight times by using various finite elements with different meshes and hyperelastic models. The results are very similar in all cases and their average is presented in Fig. 5a graphically.

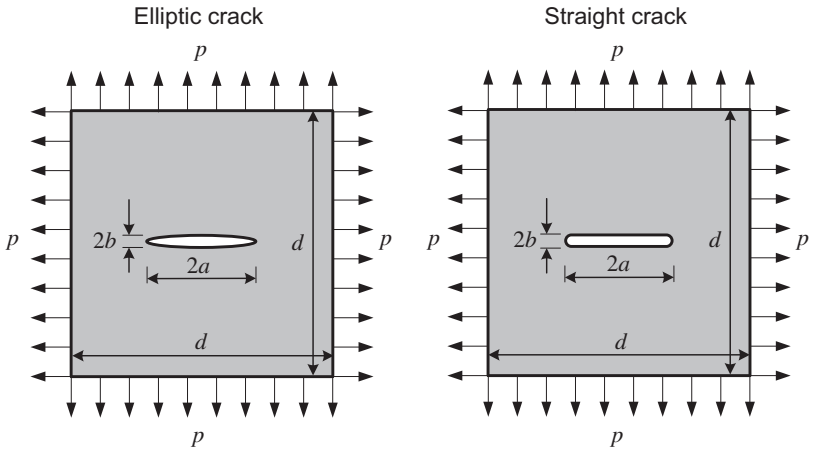

Fig. 3. Elliptic and straight cracks.

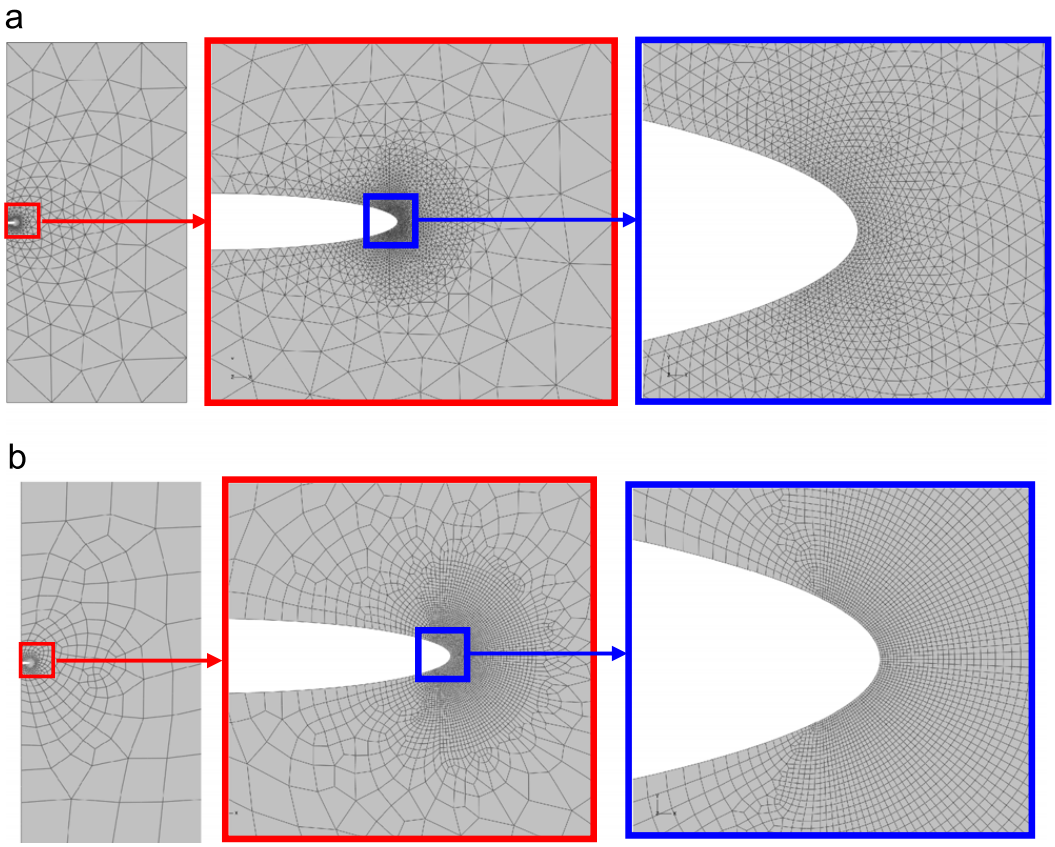

Fig. 4. Meshes of triangles (a) and quadrilaterals (b).

Table 1
Normalized critical tension, p_{cr}/Φ, for elliptic crack with varying sharpness, and fixed length

b/a	SH2						SH1	
	CPS3		CPS4		CPS8		CPS3	
1/40	2.2 (2228)	2.3 (6802)	2.3 (1251)	2.2 (3141)	2.2 (1251)	2.2 (3141)	2.0 (2228)	2.1 (6802)
2/40	4.3 (9454)	4.3 (16794)	4.3 (4305)	4.4 (9131)	4.2 (4305)	4.2 (9131)	3.8 (9454)	3.8 (16794)
3/40	6.5 (6482)	6.6 (18266)	6.6 (2626)	6.4 (8103)	6.4 (2626)	6.4 (8103)	5.6 (6482)	5.6 (18266)
4/40	8.6 (5558)	8.6 (15234)	8.7 (2532)	8.7 (6808)	8.5 (2532)	8.5 (6808)	7.5 (5558)	7.5 (15234)
5/40	10.7 (4118)	10.8 (13330)	10.9 (1963)	10.9 (5820)	10.7 (1963)	10.7 (5820)	9.5 (4118)	9.6 (13330)
6/40	12.8 (4696)	12.7 (12916)	12.9 (2285)	12.9 (5672)	12.7 (2285)	12.7 (5672)	11.3 (4696)	11.3 (12916)
7/40	14.8 (3892)	14.8 (12798)	15.1 (1886)	14.9 (5677)	14.7 (1886)	14.7 (5677)	13.2 (3892)	13.2 (12798)
8/40	16.9 (4420)	16.9 (13502)	17.2 (2124)	17.1 (6025)	16.9 (2124)	16.9 (6025)	15.0 (4420)	15.0 (13502)

SH1, softening hyperelasticity model described by Eq. (33); SH2, softening hyperelasticity model described by Eq. (30); CPS3, CPS4, CPS8, ABAQUS triangle and quadrilateral elements; parentheses designate the total number of finite elements for the half plate.

It is clearly seen that the critical tension significantly depends on the sharpness of the elliptic crack. When the critical tension is known we can calculate the material toughness by using Eq. (4):

$$K_{Ic} = p_{cr}\sqrt{\pi a}. \tag{38}$$

The results of the calculations of the material toughness are presented in Fig. 5b. Evidently, no unique toughness can be determined for a crack with the fixed length. The numerical value of the toughness depends on the sharpness of the crack.

It is worth emphasizing that the "smallness" of the crack was checked by comparing the results of the present computations to the results of the similar computations with the enlarged plate. No significant difference in results has been found and we do not duplicate them here.

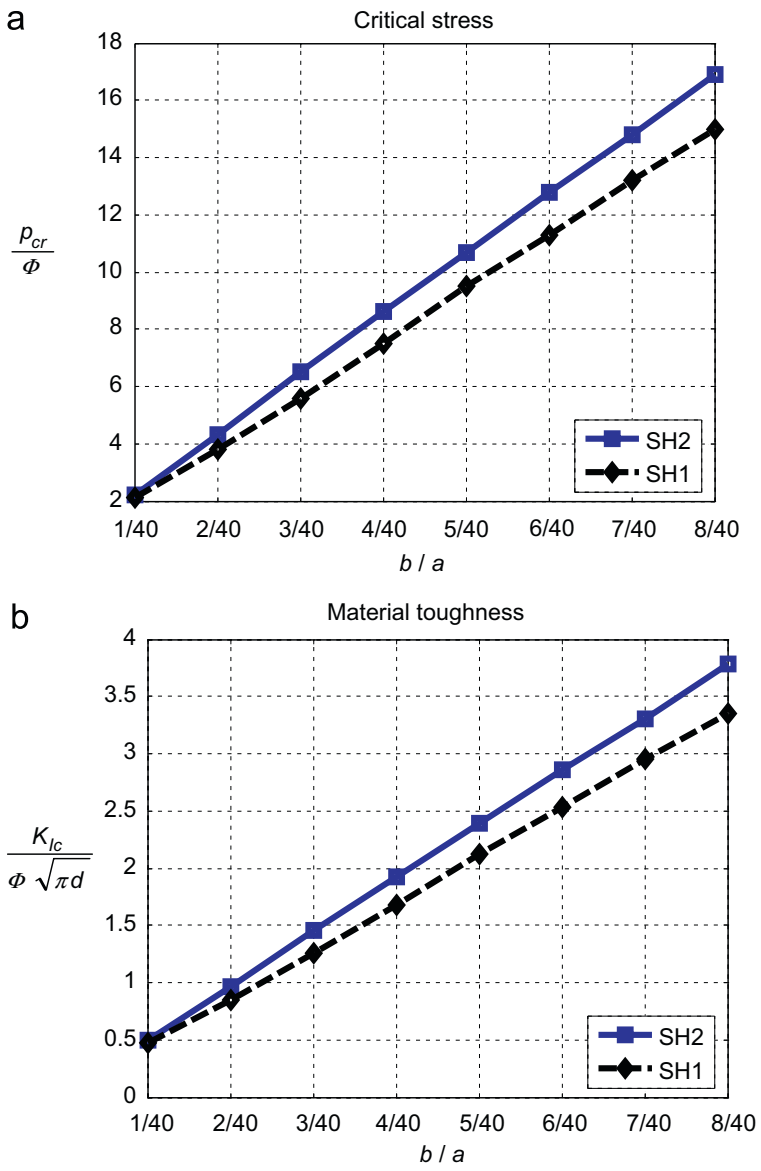

Fig. 5. Critical stress (a) and material toughness (b) for elliptic crack with varying sharpness and fixed length. SH1—softening hyperelasticity model described by Eq. (33); SH2—softening hyperelasticity model described by Eq. (30).

3.2. Straight crack with varying sharpness

The results similar to those presented in the previous subsection are also obtained for the straight crack, which is formed by two parallel lines joined by half-circles at the edges. Table 2 and Fig. 6 show the critical tensions and the material toughness for the case of the straight crack with the varying sharpness, i.e. width.

Again, like in the case of the elliptic crack, no unique magnitude of the material toughness can be determined because it depends on the crack sharpness.

3.3. Straight crack with varying length

In addition to the analysis of the influence of the crack sharpness on the critical tension of a plate, it is of interest to compare cracks with the equivalent sharpness and varying lengths. Such comparisons are presented in Table 3 and Fig. 7. The obtained data clearly show that the crack length affects the critical tension in

Table 2
Normalized critical tension, p_{cr}/Φ, for straight crack with varying sharpness and fixed length

b/a	SH2 (CPS3)		SH1 (CPS3)	
0.5/40	8.8 (1296)	9.0 (1738)	8.4 (1296)	8.6 (1738)
1/40	12.7 (1764)	12.7 (3624)	12.0 (1764)	12.0 (3624)
1.5/40	15.6 (1366)	15.7 (2694)	14.4 (1366)	14.5 (2694)
2/40	18.0 (1382)	18.1 (2546)	16.2 (1382)	16.3 (2546)
2.5/40	20.1 (1338)	20.4 (2268)	18.0 (1338)	18.3 (2268)
3/40	22.0 (1326)	22.2 (2262)	19.7 (1326)	19.9 (2262)
3.5/40	23.7 (1274)	23.8 (2298)	21.2 (1274)	21.3 (2298)
4/40	25.3 (1274)	25.5 (2368)	22.6 (1274)	22.8 (2368)

SH1, softening hyperelasticity model described by Eq. (33); SH2, softening hyperelasticity model described by Eq. (30); CPS3, ABAQUS triangle element; parentheses designate the total number of finite elements for the half plate.

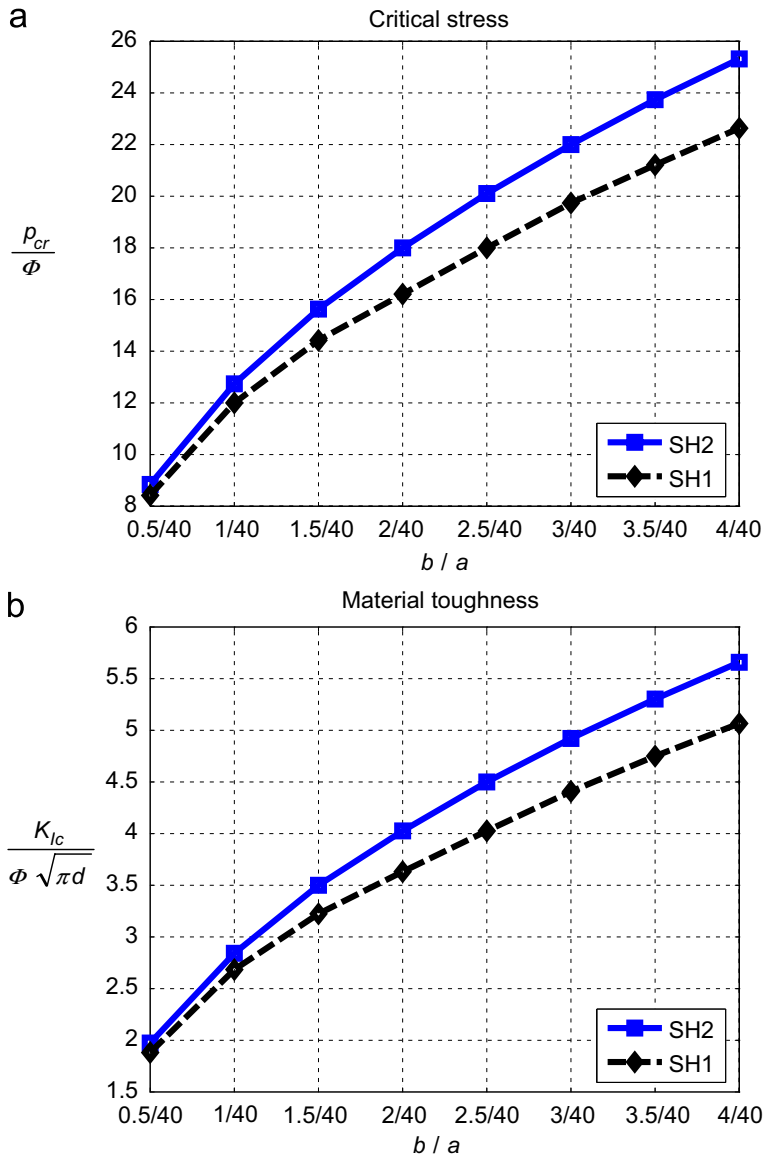

Fig. 6. Critical stress (a) and material toughness (b) for straight crack with varying sharpness and fixed length. SH1—softening hyperelasticity model described by Eq. (33); SH2—softening hyperelasticity model described by Eq. (30).

Table 3
Normalized critical tension, p_{cr}/Φ, for straight crack with constant yet different sharpness and varying length

a/b	SH2 (CPS3)		a/b	SH2 (CPS3)		a/b	SH2 (CPS3)	
10/1	25.3 (1480)	25.5 (3156)	10/2	35.1 (1050)	35.0 (2042)			
20/1	18.0 (1352)	18.0 (3068)	20/2	25.3 (1136)	25.6 (2114)	20/3	31.5 (2110)	31.7 (3698)
30/1	14.7 (1640)	14.7 (3430)	30/2	20.8 (1318)	21.0 (2356)	30/3	25.3 (2308)	25.6 (3772)
40/1	12.7 (1764)	12.7 (3624)	40/2	18.0 (1382)	18.1 (2546)	40/3	22.0 (2262)	22.1 (4040)
50/1	11.4 (1720	11.6 (2840)	50/2	16.0 (1592)	16.1 (2804)	50/3	19.9 (2610)	20.0 (4180)
60/1	10.4 (1978)	10.4 (4024)	60/2	14.6 (1687)	14.7 (2980)	60/3	18.0 (2962)	18.1 (4600)
70/1	9.5 (2190)	9.6 (4334)	70/2	13.5 (1894)	13.7 (3260)	70/3	16.8 (3052)	16.9 (4906)
80/1	8.9 (2232)	9.0 (4420)	80/2	12.6 (1960)	12.7 (3514)	80/3	15.7 (3480)	15.8 (5180)
90/1	8.4 (2448)	8.5 (4694)	90/2	11.8 (2164)	12.0 (3992)	90/3	14.7 (3248)	14.8 (5256)
100/1	7.9 (2622)	8.0 (4848)	100/2	11.2 (2262)	11.3 (3970)	100/3	13.9 (3426)	13.9 (5508)

SH2, softening hyperelasticity model described by Eq. (30); CPS3, ABAQUS triangle element; parentheses designate the total number of finite elements for the half plate.

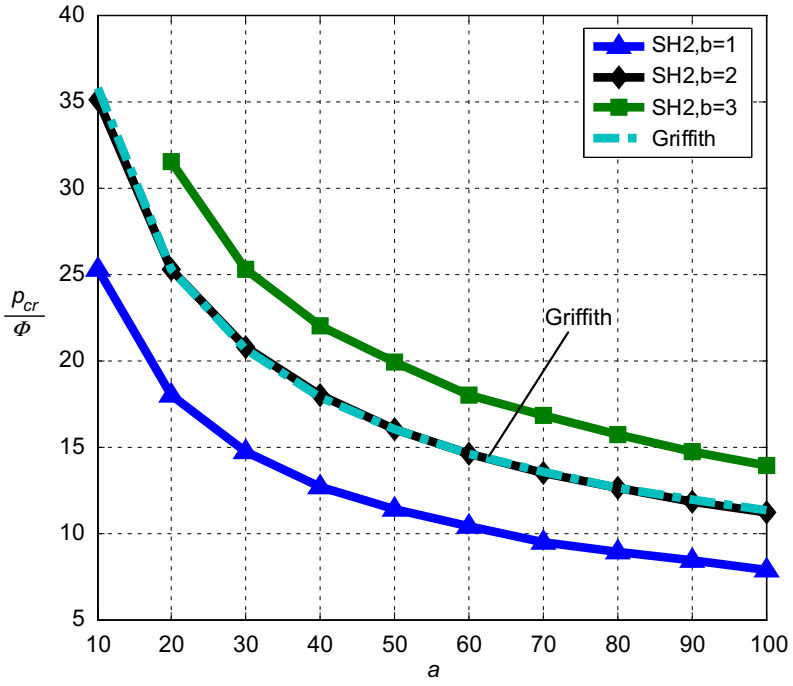

Fig. 7. Critical stress for straight crack with fixed yet different sharpness and varying length. SH2—softening hyperelasticity model described by Eq. (30). Griffith—prediction based on Eq. (4) for K_{Ic} calibrated at $a/b = 50/2$.

agreement with the Griffith theory and LEFM only in the case of the cracks with the equivalent sharpness. The latter means that if the Griffith theory and LEFM were calibrated for the sharpness corresponding to the middle curve in Fig. 7 then they could only predict the behavior of the cracks with the same sharpness and they would fail predicting the behavior of cracks with a different sharpness.

4. Discussion

The present work was motivated by a controversy between the observations of the influence of the crack sharpness on the toughness in experiments and the ignorance of the crack sharpness in the classical theories of brittle fracture. To gain new insight in the controversy, we numerically simulated the onset of the crack propagation in thin plates under the hydrostatic tension. The critical tension, when fracture starts, occurs when material fails at the tip of the crack. The failure is driven by the strain softening induced in the material

constitutive model with the help of the energy limiter—the average bond energy. The material (Hookean) model enhanced with the failure description was plugged in ABAQUS and crack simulations were performed on very fine meshes to examine the influence of the crack sharpness on the onset of fracture. Small elliptic and straight cracks were considered with constant length and varying width, i.e. the tip curvature or the crack sharpness. It was observed that sharper cracks led to lower magnitudes of the critical tension. The latter, in turn, led to the lower magnitudes of the critical SIFs—material toughness—in harmony with the experimental observations.

Our observations are in agreement with the well-known Inglis (1913) finding that the stress at the tip of an elliptic crack strongly depends on its sharpness. Assuming that the stress at the tip controls material strength, it is possible to expect that the crack sharpness affects the onset of material failure. Such a scenario was considered by Inglis using linear elasticity. Comparing the approach of Inglis with the softening hyperelasticity approach used in the present work, we should emphasize the difference between them. Inglis uses local—strength of materials—criteria of failure which are separated from the constitutive description of material. No global experiment on the calibration of the fracture toughness can be reproduced within the simplistic framework of strength of materials. The softening hyperelasticity approach is different. It allows tracking the global failure/instability of the structure with cracks due to the inclusion of the strain softening in the constitutive description of material. Thus, softening hyperelasticity allows reproducing the real physical experiments where the global instability/failure is observed. We should also note that Emmerich (2007) revisited Inglis results by mixing continuum and atomistic arguments and arriving at similar conclusions. The Emmerich (2007) work includes interesting discussions and an extensive list of references, which complements the references of the present work.

Why are the Griffith theory and LEFM ignorant of the crack sharpness? Such ignorance can be explained by the notion that the classical theories of brittle fracture are based on the energy balance considerations, which are integral and because of that they 'smear' the real stress/strain concentration at the tip of a real crack. The latter is explicit in the Griffith work where the energy balance is the basis of the theory. The energy nature of LEFM appears in disguise. Indeed, the critical SIF that indicate the onset of fracture are the coefficients in the local asymptotic expansions of stress fields. At first glance, they are not formally related to any energy consideration. However, the SIFs are "truly esoteric quantities" (Hutchinson, 2002) unless they are physically interpreted within the energetic framework of Griffith and the link is established between the critical SIF and the critical energy release rate. Thus, the fracture criteria of LEFM are essentially energetic though they appear in a form related to the local stress. It is remarkable that though the classical theories of brittle fracture ignore the crack sharpness they are capable of describing the influence of the crack length on the critical load very well in the case where the crack sharpness is constant. Our simulations of the straight cracks show that the critical tension depends inversely on the square root of the crack length in full harmony with the Griffith finding. Unfortunately, that is true only for the equivalent cracks, i.e. cracks with the same tips.

The main practical implication of our results is a conclusion that generally material toughness cannot be uniquely calibrated in experimental tests because its numerical magnitude significantly depends on the sharpness of the crack/notch used for the calibration. The crack sharpness controls the stress/strain concentration, which in turn controls the onset of fracture. It is possible, however, to decrease the radius of the tip of the crack/notch to a magnitude where our conclusion based on the classical continuum considerations is not applicable. Such a magnitude should be related with a characteristic length of the material microstructure, e.g. grain size, atomic distance, etc., corresponding, for example, to the Emmerich (2007) parameter λ_a that represents the minimum characteristic length scale round the point where the fracture begins. Concerning the latter remark, it is interesting to quote Munz and Fett (1999) who notice that the convergence of the measured fracture toughness starts with a notch radius smaller than a critical value: "For a fine-grained ceramic a very narrow notch is necessary. In all cases it has to be ensured that the saw cut is narrow enough". In our opinion, the 'narrow enough' is defined by the grain size. The said is applicable to any sort of brittle materials.

Acknowledgments

We are grateful to Prof. Huajian Gao for his remarks on the initial version of the manuscript and for drawing our attention to the work by Emmerich (2007).

This research was partly supported by Technion V.P.R. fund.

References

Barenblatt, G.I., 1959. The formation of equilibrium cracks during brittle fracture. General ideas and hypotheses. Axially-symmetric cracks. J. Appl. Math. Mech. 23, 622–636.

Belytschko, T., Moes, N., Usiu, S., Parimi, C., 2001. Arbitrary discontinuities in finite elements. Int. J. Numer. Meth. Eng. 50, 993–1013.

Bertolotti, R.L., 1973. Fracture toughness of polycrystalline Al_2O_3. J. Am. Ceram. Soc. 56, 107–110.

Broberg, K.B., 1999. Cracks and Fracture. Academic Press, London.

Camacho, G.T., Ortiz, M., 1996. Computational modeling of impact damage in brittle materials. I. J. Solids Struct. 33, 2899–2938.

De Borst, R., 2001. Some recent issues in computational failure mechanics. Int. J. Numer. Meth. Eng. 52, 63–95.

Doremus, R.H., 1976. Cracks and energy criteria for brittle fracture. J. Appl. Phys. 47, 1833–1836.

Dugdale, D.S., 1960. Yielding of steel sheets containing slits. J. Mech. Phys. Solids 8, 100–104.

Emmerich, F.G., 2007. Tensile strength and fracture toughness of brittle materials. J. Appl. Phys. 102, 073504.

Gao, H., Klein, P., 1998. Numerical simulation of crack growth in an isotropic solid with randomized internal cohesive bonds. J. Mech. Phys. Solids 46, 187–218.

Gao, H., Ji, B., Jager, I.L., Arzt, E., Fratzl, P., 2003. Materials become insensitive to flaws at nanoscale: Lessons from nature. Proc. Natl. Acad. Sci. 100, 5597–5600.

Gogotsi, G.A., 2003. Fracture toughness of ceramics and ceramic composites. Ceram. Int. 7, 777–784.

Griffith, A.A., 1921. The phenomena of rupture and flow in solids. Philos. Trans. R. Soc. Lond. A 221, 163–198.

Hellan, K., 1984. Introduction to Fracture Mechanics. McGraw-Hill, New York.

Hertzberg, R.W., 1989. Deformation and Fracture of Engineering Materials, third ed. Wiley.

Hutchinson, J.W., 2002. Life as a mechanician: 1956-. Timoshenko Medal Acceptance Speech: 〈http://imechanica.org/node/195〉.

Inglis, C.E., 1913. Stresses in a plate due to presence of cracks and sharp corners. Proc. Inst. Nav. Archit. 55, 219–241.

Ji, B., Gao, H., 2004. A study of fracture mechanisms in biological nano-composites via the virtual internal bond model. Mater. Sci. Eng. A 366, 96–103.

Kachanov, L.M., 1958. Time of the rupture process under creep conditions. Izv. Akad. Nauk SSSR, Otdelenie Teckhnicheskikh Nauk 8, 26–31.

Kachanov, L.M., 1986. Introduction to Continuum Damage Mechanics. Martinus Nijhoff Dotrecht, The Netherlands.

Kanninen, M.F., Popelaar, C., 1973. Fundamentals of Fracture Mechanics. Butterworth, London.

Klein, P., Gao, H., 1998. Crack nucleation and growth as strain localization in a virtual-bond continuum. Eng. Fract. Mech. 61, 21–48.

Krajcinovic, D., 1996. Damage Mechanics. Elsevier, North Holland Series in Applied Mathematics and Mechanics.

Lemaitre, J., Desmorat, R., 2005. Engineering Damage Mechanics: Ductile, Creep, Fatigue and Brittle Failures. Springer, Berlin.

Munz, D., Fett, T., 1999. Ceramics: Mechanical Properties, Failure Behaviour, Material Selection. Springer, Berlin.

Munz, D., Bubsey, R.T., Shannon, J.L., 1980. Fracture toughness determination of Al2O3 using four point bend specimens with straight-through and chevron notches. J. Am. Ceram. Soc. 63, 300–305.

Myers, R.J., Hillberry, B.M., 1977. Effect of notch radius in the fracture behavior of mono-crystalline silicon. In: ICF4 Proceedings, vol. 3. Waterloo, Canada, pp. 1001–1005.

Needleman, A., 1987. A continuum model for void nucleation by inclusion debonding. J. Appl. Mech. 54, 525–531.

Rabotnov, Y.N., 1963. On the equations of state for creep. In: Progress in Applied Mechanics (Prager Anniversary Volume). MacMillan, New York.

Rice, J.R., Wang, J.S., 1989. Embrittlement of interfaces by solute segregation. Mater. Sci. Eng. A 107, 23–40.

Rittel, D., Wang, Z.G., Merzer, M., 2006. Adiabatic shear failure and dynamic stored energy of cold work. Phys. Rev. Lett. 96, 075502.

Skrzypek, J., Ganczarski, A., 1999. Modeling of Material Damage and Failure of Structures. Springer, Berlin.

Tadmor, E.B., Ortiz, M., Phillips, R., 1996. Quasicontinuum analysis of defects in solids. Philos. Mag. 73, 1529–1563.

Tsuji, K., Iwase, K., Ando, K., 1999. An investigation into the location of crack initiation sites in alumina, polycarbonate and mild steel. Fatigue Fract. Eng. Mater. Struct. 22, 509–517.

Tvergaard, V., Hutchinson, J.W., 1992. The relation between crack growth resistance and fracture process parameters in elastic-plastic solids. J. Mech. Phys. Solids 40, 1377–1397.

Volokh, K.Y., 2004. Nonlinear elasticity for modeling fracture of isotropic brittle solids. J. Appl. Mech. 71, 141–143.

Volokh, K.Y., 2007a. Softening hyperelasticity for modeling material failure: analysis of cavitation in hydrostatic tension. Int. J. Solids Struct. 44, 5043–5055.

Volokh, K.Y., 2007b. Hyperelasticity with softening for modeling materials failure. J. Mech. Phys. Solids 55, 2237–2264.

Volokh, K.Y., Gao, H., 2005. On the modified virtual internal bond method. J. Appl. Mech. 72, 969–971.

Volokh, K.Y., Ramesh, K.T., 2006. An approach to multi-body interactions in a continuum-atomistic context: application to analysis of tension instability in carbon nanotubes. Int. J. Solids Struct. 43, 7609–7627.

Wang, J., Rainforth, W.M., Wadsworth, I., Stevens, R., 1992. The effects of notch width on the SENB toughness for oxide ceramics. J. Eur. Ceram. Soc. 10, 21–31.

Weiner, J.H., 1983. Statistical Mechanics of Elasticity. Wiley, New York.

Xu, X.P., Needleman, A., 1994. Numerical simulations of fast crack growth in brittle solids. J. Mech. Phys. Solids 42, 1397–1434.

Yosibash, Z., Bussiba, A., Gilad, I., 2004. Fracture criteria for brittle elastic materials. Int. J. Fract. 125, 307–333.

Zhang, P., Jiang, H., Huang, Y., Geubelle, P.H., Hwang, K.C., 2004. An atomistic-based continuum theory for carbon nanotubes: analysis of fracture nucleation. J. Mech. Phys. Solids 52, 977–998.